

Article

# Exploring the Difference in Bainite Transformation with Varying the Prior Austenite Grain Size in Low Carbon Steel

Liangyun Lan <sup>1,2,\*</sup> , Zhiyuan Chang <sup>3</sup> and Penghui Fan <sup>1</sup>

<sup>1</sup> School of Mechanical Engineering and Automation, Northeastern University, Shenyang 110819, China; 1600335@stu.neu.edu.cn

<sup>2</sup> Key Laboratory of Vibration and Control of Aero-Propulsion Systems, Ministry of Education of China, Northeastern University, Shenyang 110819, China

<sup>3</sup> State key Laboratory of Rolling Technology and Automation, Northeastern University, Shenyang 110819, China; changzyhpu@163.com

\* Correspondence: lanly@me.neu.edu.cn; Tel.: +86-248-367-4140

Received: 2 November 2018; Accepted: 21 November 2018; Published: 24 November 2018



**Abstract:** The simulation welding thermal cycle technique was employed to generate different sizes of prior austenite grains. Dilatometry tests, in situ laser scanning confocal microscopy, and transmission electron microscopy were used to investigate the role of prior austenite grain size on bainite transformation in low carbon steel. The bainite start transformation ( $B_s$ ) temperature was reduced by fine austenite grains (lowered by about 30 °C under the experimental conditions). Through careful microstructural observation, it can be found that, besides the Hall–Petch strengthening effect, the carbon segregation at the fine austenite grain boundaries is probably another factor that decreases the  $B_s$  temperature as a result of the increase in interfacial energy of nucleation. At the early stage of the transformation, the bainite laths nucleate near to the grain boundaries and grow in a “side-by-side” mode in fine austenite grains, whereas in coarse austenite grains, the sympathetic nucleation at the broad side of the pre-existing laths causes the distribution of bainitic ferrite packets to be interlocked.

**Keywords:** low carbon steel; prior austenite grain boundary; carbon segregation;  $B_s$  temperature

## 1. Introduction

Prior austenite grain size is a vitally important parameter to influence phase transformation behavior in steels, because to a great extent, it determines the number of nucleation sites and the space of the growth of products. For martensite transformation, it is well recognized that fine prior austenite grain size decreases the martensite start transformation ( $M_s$ ) temperature, as the Hall–Petch strengthening effect for fine austenite grains improves resistance to the plastic deformation of martensite transformation [1]. Meanwhile, it further refines the martensitic block width and packet size, or likely forms a phenomenon of variant selection in the crystallography, which plays a critical role in tailoring the final mechanical properties [2–5].

The effect of prior austenite grain size on bainite transformation is also of significance, although the related results seem to be in dispute [6–11]. Some studies considered that fine austenite grains accelerate the kinetics of bainite transformation, as the increase in the number of grain boundaries provides more preferable sites for nucleation of ferritic laths. By contrast, others found that the bainite formation is insensitive to the prior grain size or even that the growth of bainite is retarded by fine prior grains. The bainite start transformation ( $B_s$ ) temperature is found to be lowered with decreasing austenite grain size under the continuous cooling condition, a very similar trend to that found with the  $M_s$  temperature. It is taken for granted that they have a similar mechanism for the decrease in

transformation temperature [10,11]. However, it should be noted that the martensite transformation is an athermal transformation, whereas the bainite transformation is, sometimes, regarded as a kind of thermally activated nucleation and growth reaction—it does not seem very convincing that the Hall–Petch strengthening effect in fine austenite grains is considered as a sole factor to decrease the  $B_s$  temperature. Recently, some studies reported that the variant distribution of bainite is limited in fine austenite grains compared with large austenite grains [12–14]. This phenomenon may be related to the difference in the temperature range of bainite transformation with varying prior grain size [13]. It is thus worth further exploring what else, besides the Hall–Petch strengthening effect, is likely to play a role in retarding the bainite transformation for fine austenite grains.

In this work, welding thermal simulation was employed to generate different sizes of prior austenite grains and to prove the effect of prior grain size on phase transformation, because the inhomogeneous austenite grain size is representative of the heat-affected zone (HAZ). In situ observation using high-temperature laser scanning confocal microscopy (LSCM) and partial bainite transformation tests were carried out to further reveal the microstructural characters at the early stage of the transformation with different prior austenite grain sizes.

## 2. Experimental Method

The chemical composition of low carbon steel in this study was 0.053 C, 0.22 Si, 1.35 Mn, 0.082 (Nb + V + Ti), 0.0012 B, 0.23 Cr, 0.37 Mo balanced by Fe.

Specimens with dimensions of  $\phi 6 \times 50$  mm were cut from the hot rolled steel plate along the transversal direction. The HAZ simulations were carried out using a thermo-mechanical simulator and a two dimensional Rykalin mathematical model was adopted to control the testing temperature. A Pt-10% Rh thermocouple was welded at the middle of the cylinders to monitor the temperature change during heat treatment. A linear variable displacement transducer type dilatometer was used to measure the relative change in diameter of these samples.

Specimens were heated to a peak temperature at a rate of  $130 \text{ }^\circ\text{C/s}$  and held for 2 s. The peak temperature was set at 1350 and  $1100 \text{ }^\circ\text{C}$  to obtain widely varying austenite grain sizes, which simulates the thermal cycles at coarse grained HAZ (CGHAZ) and fine grained HAZ (FGHAZ), respectively. The samples were then subjected to various cooling rates that were defined as the cooling time from 800 to  $500 \text{ }^\circ\text{C}$  (the  $t_{8/5}$  time varies from 5 to 600 s) until the phase transformation has completed. Figure 1 shows the measured thermal cycle curves. Dilatation curves were obtained to determine the phase change temperatures. Continuous cooling transformation (CCT) diagrams for the CGHAZ and FGHAZ were constructed together to exhibit the effect of prior austenite grain size on phase transformation, although the CCT diagram of the CGHAZ has been reported elsewhere [13].

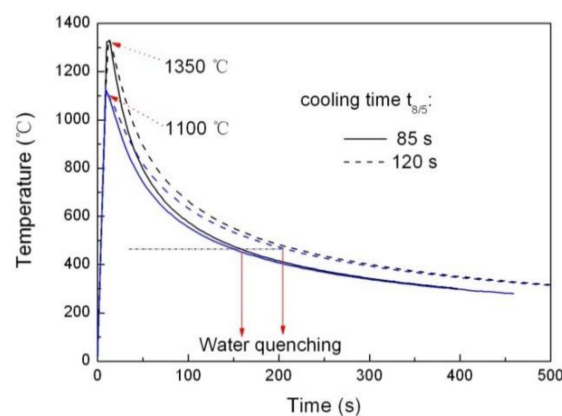


**Figure 1.** Typical thermal cycle curves with different peak temperatures and cooling times (water quenching process signified schematically with red arrows).

The partially transformed bainite microstructure was expected to be retained using an interrupted cooling method by water quenching. Based on the CCT diagrams, the partial bainite transformation samples were quenched in water immediately after the welding thermal cycle temperature was lowered to 470, 500, or 550 °C, as signified with red arrows in Figure 1.

For in situ observation of phase transformation, two samples were cut directly from the welding thermal simulation samples, machined into disks (6 mm diameter and 3 mm thickness), and then mechanically polished. These prepared samples were austenitized at 1300 °C and 1100 °C to simulate the CGHAZ and FGHAZ thermal cycles, respectively. The linear cooling rate of 2.5 °C/s was employed, which is approximately equal to the average cooling rate of the  $t_{8/5} = 120$  s cooling time. The real-time information of phase transformation was recorded using high-temperature LSCM.

Metallographic specimens were cut from the heat treatment region of interest and then polished by conventional techniques. Microstructural characteristics were examined using an optical microscope (Leica DMIRM, Leica company, Weitz, Germany), a field-emission scanning electron microscope equipped with electron probe microanalysis (SEM, ULTRA 55, ZEISS, Jena, Germany), and a transmission electron microscope (TEM, FEI Tecnai G<sup>2</sup>F20, FEI company, Hillsboro, OR, USA). Vickers hardness measurements were conducted using an FM 700 hardness-testing machine (Hardness tester, FM-700, FUTURE-TECH company, Kawasaki-City, Japan) employing a 0.5 N load with 15 s dwell time. The average hardness values for each heat treatment condition were calculated based on at least 10 repeat tests.

### 3. Results and Discussion

On the basis of the dilatation curves (some typical examples were given in the literature [11,13]), the transformation start/finish temperatures could be confirmed with a normal extrapolation method [15]. The CCT diagrams for CGHAZ and FGHAZ are constructed together in Figure 2a. The transformation start temperature gradually lowers and the transformation finish temperature first increases, but then decreases with the decrease in cooling time. The bainite microstructure could be formed within a wide range of cooling rates, as marked in the diagram, which are attributed to the fact that the combined addition of multi-microalloys, such as Mo, Nb, Ti, and V, into steel extends the range of bainite transformation [16]. As expected, FGHAZ always has a lower  $B_s$  temperature than CGHAZ for any given cooling rate (highlighted with gray background), although the discrepancy in bainite transformation finish temperature seems to be very insignificant. The largest difference in the  $B_s$  temperature between CGHAZ and FGHAZ is about 30 °C at the middle cooling rate.

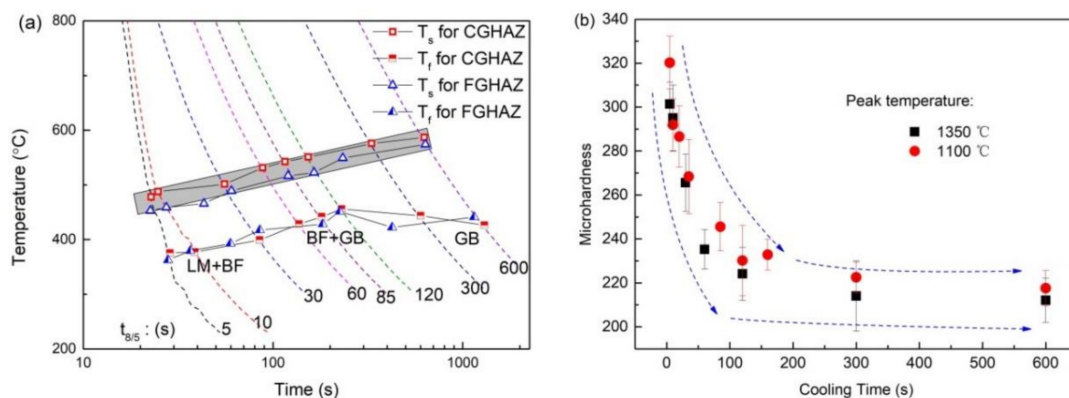


**Figure 2.** (a) Continuous cooling transformation (CCT) diagrams with different peak temperatures and (b) the change of Vickers hardness as a function of cooling time (CGHAZ: coarse grained heat-affected zone, FGHAZ: fine grained HAZ, LM: lath martensite, BF: bainitic ferrite, GB: granular ferrite).

Figure 2b shows the change of hardness with cooling time. As the cooling time increases, the hardness decreases rapidly and then gradually levels off. Meanwhile, at a given cooling rate, FGHAZ

always seems to have a slightly higher hardness than CGHAZ. This further proves the difference in transformation behaviors (Figure 2a) because the lower temperature transformation microstructure normally results in a higher hardness.

Figure 3 represents three groups of typical microstructures for CGHAZ and FGHAZ after they were subjected to the  $t_{8/5}$  times of 5, 85, and 600 s, respectively. The average grain size of FGHAZ measured with the line intercept method ranges from about 16.8  $\mu\text{m}$  to 29.5  $\mu\text{m}$ , while CGHAZ has an average grain size higher than 300  $\mu\text{m}$ . At the shortest cooling time, the microstructure is predominantly lath martensite, accompanied by very little bainitic ferrite, regardless of peak temperature (Figure 3a,d). Comparing Figure 3a and d, the packet size of martensite in the morphology seems to be refined by the fine prior grain size (Figure 3e). Because of the hierarchical structure of martensite [2–5], the block size and lath width may be also decreased in FGHAZ.

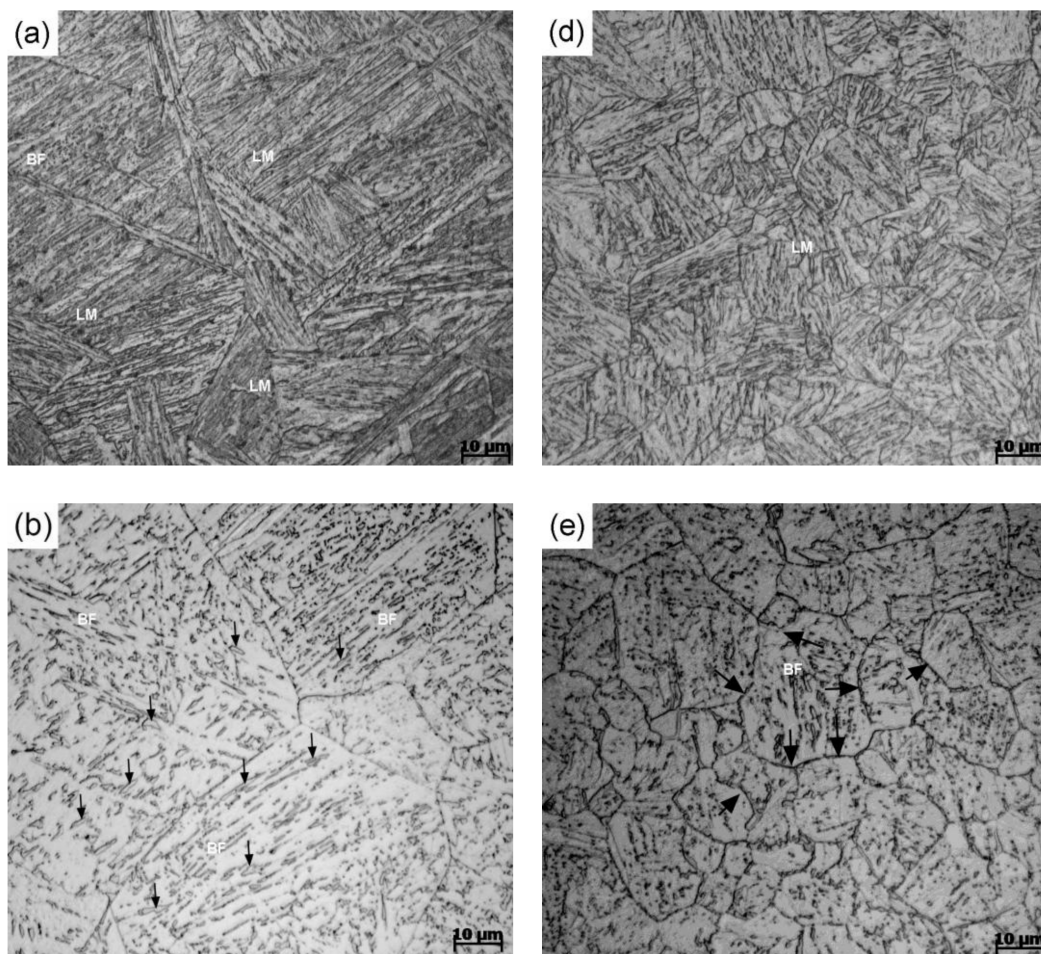
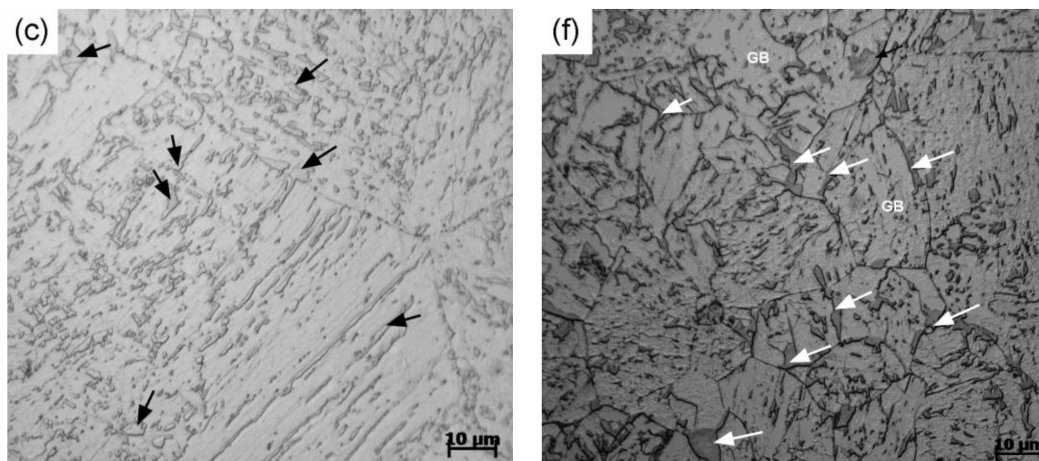


Figure 3. Cont.



**Figure 3.** Optical microstructure with different peak temperatures: (a–c) 1350 °C and (d–f) 1100 °C, and different cooling times:  $t_{8/5}$  (a,d) 5 s, (b,e) 85 s, and (c,f) 600 s. (LM: lath martensite, BF: bainitic ferrite, GB: granular ferrite, and some martensite–austenite (MA) constituents were signified with arrows).

At the cooling time (85 s), CGHAZ and FGHAZ microstructures are mainly characterized by bainitic ferrite (Figure 3b,e). However, the martensite–austenite (MA) constituents that are formed below the  $M_s$  temperature as a result of incomplete bainite transformation [17] have different sizes and distribution sites, although most of them have a similar short and slender shape. For example, the MA constituents in CGHAZ are present inside the grains and their distribution approximately describes some sites of parallel lath boundaries [17]; while in FGHAZ, most of them appear along the prior austenite grain boundaries (signified with arrows in Figure 3e), which seems to make the grain boundaries coarser. The distribution of MA constituents implies that the redistribution of carbon atoms is different during the transformation for CGHAZ and FGHAZ, because notable enrichment of carbon was observed within the MA constituents using atom probe tomography (APT) [18].

As the cooling time increases to 600 s, the predominant microstructure for CGHAZ and FGHAZ becomes granular bainite (Figure 3c,f). The MA constituents have a massive shape, mainly because the uphill diffusion of carbon atoms becomes much easier at the lower cooling rate condition [19]. However, for CGHAZ, most massive MA constituents distribute uniformly in the matrix, except that a few of the MA constituents appear along the prior austenite grain boundaries, whereas in FGHAZ, they seem to have a larger average size and are mainly attached to the grain boundaries, as signified by arrows in Figure 3c,f. Because CGHAZ and FGHAZ have similar microstructures, the difference of MA constituents should be mainly attributed to the number of grain boundaries (i.e., prior austenite grain size), as the grain boundary has a higher diffusivity for interstitial atoms (including C, B, and H) than the grain interior and also act as a sink for these atoms [20–22].

Using the high temperature LSCM observation, the real-time features of bainite at the early stage of the transformation were recorded, as shown in Figures 4 and 5. The phase transformation does not occur when the temperature decreases to 634 °C (Figure 4a). The first ferritic lath can be found at 632 °C and its nucleation site is exactly on the grain boundary, as signified with an arrow in Figure 4b. However, this temperature is higher than that detected using a dilatometer (Figure 2a). This difference is probably acceptable as the dilatometer sensitivity is about 10 percent volume fraction transformed and the free surface effect of the LSCM sample can enhance the transformation temperature [23]. With a further slightly decreasing temperature (629 °C), several ferritic laths form, simultaneously attached to the grain boundaries (Figure 4c). Meanwhile, it is very interesting to find that a newly formed ferritic lath sympathetically nucleates on the pre-existing ferritic lath and grows toward the other direction, as marked with a cycled white arrow. This mechanism is a necessity that gives rise to the interlocked distribution of bainitic ferrite packets and partitions the coarse austenite grains into several finer and separate regions [24]. Nevertheless, other grains still do not occur in phase transformation,

which means the bainite formation is inhomogeneous at the grain scale. This agrees well with the results by Sainis et al. [25], who found that the rate of nucleation varies markedly between different austenite grains.

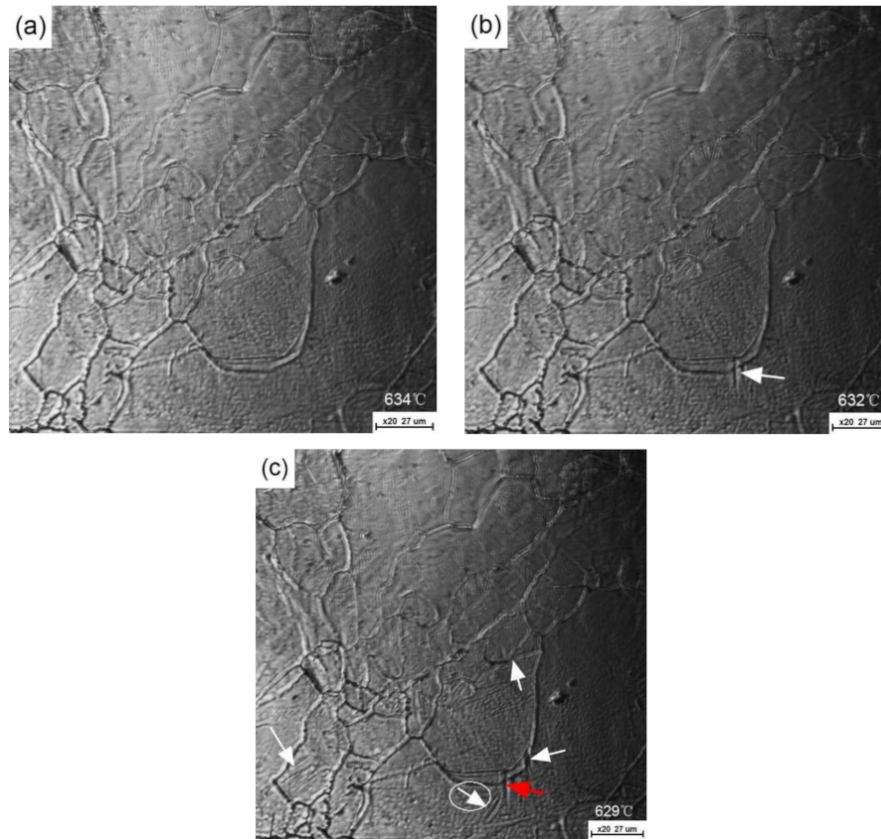


**Figure 4.** In situ observation of phase transformation with the CGHAZ thermal cycle: (a) 634 °C, (b) 632 °C, and (c) 629 °C. (The white arrows show that the ferritic laths form at the moment of real-time photographing for each image, the red arrows show the pre-existing ferritic laths.)

For the FGHAZ thermal cycle, the austenite grains are smaller and their size is more uniform (Figure 5a) compared with that of CGHAZ. When the temperature decreases to 610 °C, no obvious phase transformation takes place (Figure 5b). The ferritic laths can first be found at 605 °C, and their nucleation sites are also derived from the austenite grain boundaries (arrowed in Figure 5c), although the image quality was not as good as before. The growth rate of these ferritic laths seems to be very fast, leading to their length across almost the prior austenite grain in no time. Subsequently, the newly formed bainitic laths appear in a “side-by-side” mode relative to the pre-existing laths, rather than an interlocked mode as in CGHAZ with the decrease in temperature (Figure 5d), indicating that this mode may make only a packet structure in the morphology formed inside each fine prior austenite grain [14]. According to these real-time micrographs, it is confirmed that the fine austenite grain size decreases the  $B_s$  temperature by about 30 °C, which is in good agreement with the dilatation tests.

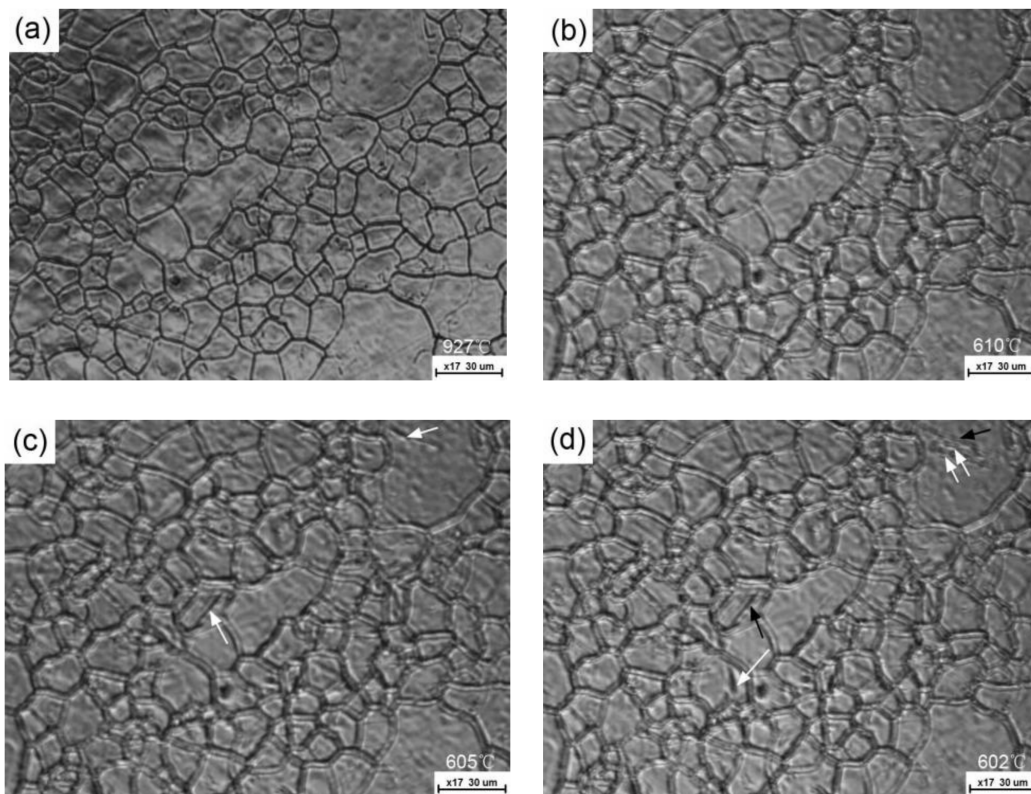


**Figure 5.** In situ observation of phase transformation with the FGHAZ thermal cycle: (a) 927 °C, (b) 610 °C, (c) 605 °C, and (d) 602 °C. (The white arrows show that the ferritic laths form at the moment of real-time photographing for each image, the black arrows show the pre-existing ferritic laths.)

Figure 6 shows the partially transformed bainite microstructure after the samples were subjected to partial welding thermal cycle cooling, followed by water quenching. At the very beginning of phase transformation, the lath morphology of ferrite forms and the nucleation of these ferritic laths are attached to the grain boundary (Figure 6a). With the progress of bainite transformation (Figure 6b), the packet structure of bainite can clearly be found as the carbides or MA constituents decorate the parallel lath boundaries. Several primary ferritic laths nucleate at different sites of the grain boundary inside one large prior austenite grain (marked with black arrows in Figure 6b), and many secondary laths sympathetically nucleate on the pre-existing ferritic laths (signified with white arrows), which agrees well with the LSCM results (Figure 4c). Through close observation of the nucleation sites of the primary laths, no MA constituents can be found, implying that in this case, the carbon atoms do not enrich at the nucleation sites of the prior austenite grain boundaries. On the contrary, most of carbon atoms should be expelled into the lath boundaries during transformation.

Only a small amount of bainite microstructures can be found for the FGHAZ sample (Figure 6c) when the quenching temperature decreases to 500 °C. The prior austenite grain boundaries seem to be particularly evident (arrowed in Figure 6c) compared with these in Figure 6a using the same etchant solution. The lath boundaries of bainite in the vicinity of prior austenite grain boundaries are ambiguous as almost no any carbide was formed to decorate these lath boundaries in these micro-regions (Figure 6d). An electron probe microanalysis on carbon distribution along the AB line (Figure 6d) across a prior austenite grain boundary semi-quantitatively shows that the prior austenite grain boundary with MA constituent contains much higher carbon concentration compared with the grain interior (Figure 6e).

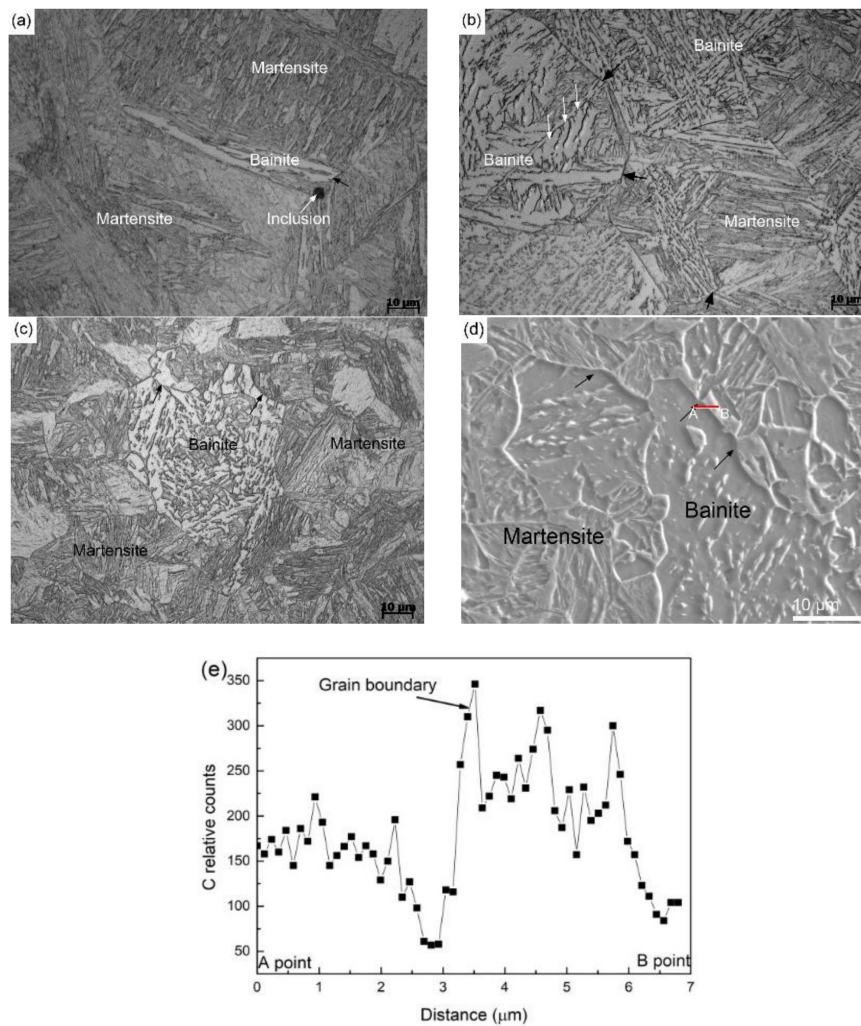


**Figure 6.** Partially transformed bainite microstructure obtained by water quenching: (a,b) peak temperature of 1350 °C with 85 °C/s cooling rate and quenching temperatures of 550 °C and 500 °C, respectively; (c,d) peak temperature of 1100 °C with 120 °C/s cooling rate and quenching temperatures of 500 °C and 470 °C, respectively; (e) the carbon distribution along the AB line across one grain boundary shown in (d).

Several TEM images were joined together in Figure 7 to show the morphology of bainite formed inside a fine prior austenite grain. Each of ferritic laths seem to be composed of several sub-units (one of which was delineated) and very few of MA constituents can be formed along the lath boundaries. These features are different from the morphology of bainite formed in coarse prior austenite grains (the lath boundaries are always decorated by the slender MA constituents shown in Figure 5d of the literature [13]). Based on the bainite transformation theory, these sub-units formed with a limited size may be attributed to the fact that the increase in strength of austenite due to a relatively lower transformation temperature or the limited space of ferritic growth impedes the plastic accommodation of remaining austenite for transformation strain [26].

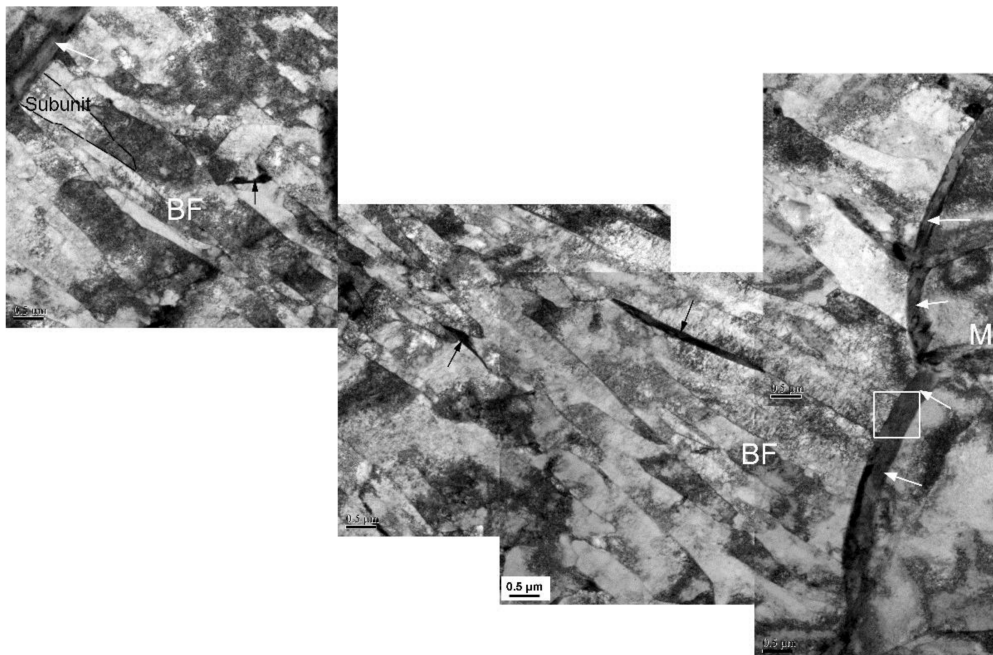


**Figure 7.** Transmission electron microscope (TEM) images showing the fine structure and grain boundary character of partially transformed microstructure using the same sample of Figure 6d (BF: bainitic ferrite, M: martensite, grain boundary MA constituents are signified with white arrows and fine MA constituents are marked with black arrows).

Most interestingly, the prior grain boundaries are decorated by many long strip MA constituents with an average width of about  $0.4 \mu\text{m}$ , as signified with white arrows (Figure 7). The magnified image in Figure 8 shows they have a character of high density dislocation martensite, which implies that the austenite along the grain boundaries is stabilized by carbon enrichment at these micro-zones, and most of them transform into martensite during final quenching. From the morphology of ferritic lath point of view, these carbon atoms enriched at the grain boundaries are considered to occur in super-cooled austenite at very early stages of the transformation or even prior to the transformation. Assuming that these segregated carbon atoms are expelled from the product phase during the transformation, they should be enriched in front of the phase interface and a quasi-eutectoid structure is likely to be formed [27], as presented in CGHAZ.

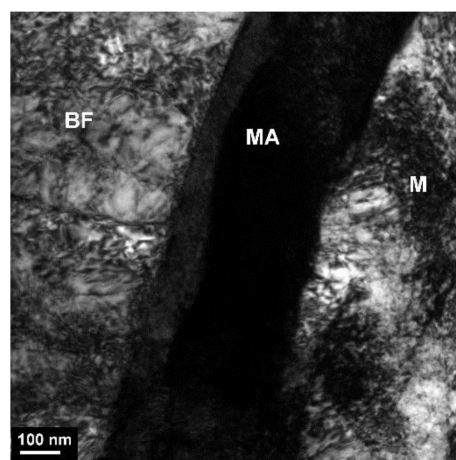


**Figure 8.** The magnified image showing the fine structure of the grain boundary MA constituent corresponding to the zone squared in Figure 7 (BF: bainitic ferrite, MA: grain boundary MA constituent, M: martensite that transformed from remaining austenite of neighboring grain).

#### 4. Overall Discussion

The size and distribution of MA constituents are different between CGHAZ and FGHAZ, regardless of similar microstructures under any cooling time condition (e.g., Figures 3 and 6). This means that the prior austenite grain size to some extent influences the redistribution of carbon atoms before and after the transformation, as schematically shown in Figure 9. The distribution of carbon atoms should be very uniform in CGHAZ grains at elevated temperatures (Figure 9a), as the solid solubility of carbon in austenite increases with the temperature. Additionally, the number of vacancies generated inside the grains increases with the temperature, and they bind with carbon atoms to form stable carbon–vacancy pairs [20,28]. As a result, the carbon atoms uniformly distribute in super-cooled austenite for CGHAZ. During the transformation, the excess carbon atoms for BCC crystals are expelled in front of the phase interface into the lath boundaries (Figure 9b).

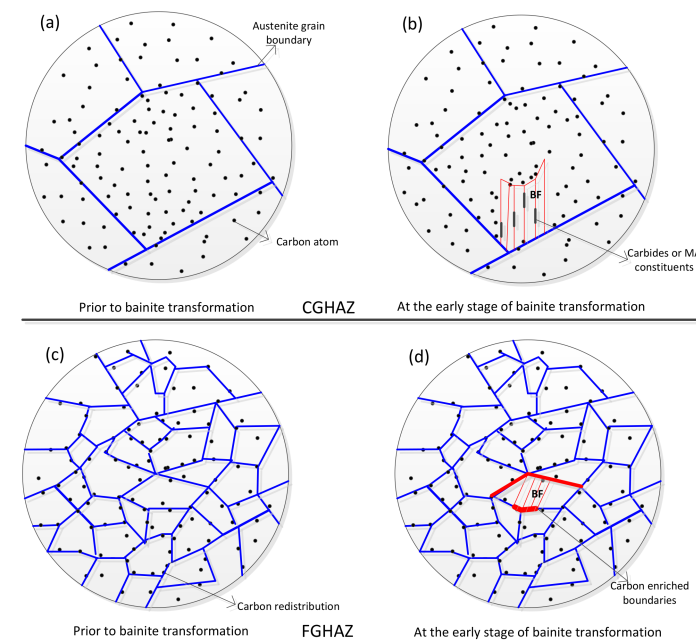


**Figure 9.** Carbon redistribution in super-cooled austenite before and after the onset of bainite transformation for CGHAZ (a,b) and FGHAZ (c,d).

The carbon atoms segregated along the prior austenite grain boundaries for FGHAZ (Figure 9c) may be derived from the following two reasons. First, the grain boundary acts as a sink for vacancies. The higher the density of grain boundaries, the easier the grain boundary segregation of carbon atoms occurs because of the equilibrium and non-equilibrium segregation mechanism [29]. Second, the trend of carbon diffusion into the grain boundaries may be enhanced as a result of the lowering solid solubility of carbon in super-cooled austenite. However, the distance of carbon diffusion in FGHAZ is much shorter than in CGHAZ, and the carbon diffusivity along the grain boundary is higher than inside the grains [22], which gives rise to the presence of carbon enrichment at the grain boundaries for the FGHAZ (Figure 9c), and the grain boundaries were finally decorated with the MA constituents (Figure 9d). Timokhina et al. [30] found that two types of the remaining austenite with different lattice parameters are present as a result of different carbon content at the beginning of the transformation using an in situ neutron diffraction technique. This means that the carbon redistribution does occur at the very early stage of the transformation, which seems to be in support of our result that the carbon atoms may be segregated at the prior grain boundaries prior to the transformation, although the present steel used has a much lower carbon content.

Zhang et al. [20] considered that the prior austenite grain boundaries, which are high-energy regions with disordered atomic arrangements, could accommodate a number of carbon atoms and

thus decrease the overall energy. In this sense, the difference in the carbon concentration of the grain boundary will change the overall boundary energy, which further influences the drive force of grain boundary nucleation. Therefore, carbon segregation at the grain boundaries in FGHAZ mentioned above is probably responsible for the difference in Bs temperature. More details are discussed below.

According to the classical nucleation theory, the free energy  $\Delta G$  for nucleation at prior austenite grain boundaries is given by [31,32]

$$\Delta G = \Delta G_{\text{chem}} + [\Delta G_{\text{str}} + \Delta G_{\text{int}}] \quad (1)$$

where  $\Delta G_{\text{chem}}$  is the molar chemical Gibbs energy difference between the parent and product phase,  $\Delta G_{\text{str}}$  is the summation of molar strain energy resulting from the volume misfit between ferrite and austenite (i.e., transformation strain), and  $\Delta G_{\text{int}}$  is the molar interfacial energy for the new phase formed. The latter two items are the resistance to phase transformation. If the transformation strain can be accommodated by the plastic deformation of austenite, the required strain energy for the creation of a new nucleus is much lower. The grain boundary nucleation thus occurs under the low transformation driving force condition, as presented in CGHAZ. However, the plastic accommodation in fine austenite grains is largely constrained by the Hall–Petch strengthening effect. As a result, it is always considered to be the main factor to decrease the Bs and Ms temperatures [1,3,10,23], because a larger super-cooled temperature is required to proceed to the phase transformation.

Very little strain energy seems to be required at the early stage of the bainite transformation as the transformation strain is insignificant at this point [30]. Here, the change of interfacial energy probably plays a vital role in decreasing Bs temperature as a result of carbon segregation at the grain boundary. The heterogeneous nucleation attached to the grain boundary is mainly attributed to the fact that the prior grain boundary energy decreases the interfacial energy of new-phase nucleation. Song et al. [32] showed that the maximum reduction of interfacial energy can be achieved when the embryo forms at the high-energy austenite grain boundary. However, the austenite grain boundary energy will be reduced if the excess carbon atoms are segregated on them, leading to the fact that the energy assisting the new-phase nucleation is lowered. Madariaga et al. [33] also considered that grain boundary segregation has an influence on new-phase nucleation through the associated change of the interfacial energy and, presumably, of the structure of the boundary itself. On the basis of the partially transformed microstructure (Figure 8), the width of carbon enriched micro-zones at grain boundaries is around 0.4  $\mu\text{m}$  in FGHAZ. This means that the actual nucleation sites of ferritic laths are some distance (maybe about 0.2  $\mu\text{m}$ ) away from the grain boundaries. The nucleation of ferritic laths might not even take advantage of the prior austenite grain boundary energy. Therefore, it can be concluded that compared with CGHAZ, a larger driving force of transformation is needed to offset the increase in interfacial energy of nucleation for FGHAZ, which is embodied in the lower in Bs temperature.

## 5. Conclusions

The effect of austenite grain size on the bainite transformation, especially on the Bs temperature, was investigated under the simulation welding thermal cycle condition. Through detailed microstructural characterization and in situ observation of the early stage of phase transformation, the main findings can be given below.

- (1) The predominantly bainite microstructure can be obtained over a very wide range of cooling rates for this studied steel. The hardness decreases rapidly and then gradually levels off with the decrease in cooling rate and FGHAZ always results in a slightly higher hardness than the CGHAZ at any given cooling rate.
- (2) For a given cooling condition, FGHAZ always has a lower Bs temperature than CGHAZ, which is proven by in situ LSCM observation and partial bainite transformation tests. The prior austenite grain boundaries were always decorated by many long strip MA constituents in FGHAZ, indicating that the carbon segregation occurred at the early stage of bainite transformation.

Besides the Hall–Petch strengthening effect in FGHAZ, the increasing interfacial energy for the grain boundary nucleation due to carbon enrichment is probably another factor that lowers the Bs temperature.

- (3) A large bainitic ferrite packet can be transformed only in fine austenite grains because the ferritic laths grow in a “side-by-side” mode, although each of the laths may consist of several sub-units. In contrast, the interlocked distribution of bainitic ferrite packets can frequently be found in coarse austenite grains, which is attributed to the mechanism of sympathetic nucleation.

**Author Contributions:** Conceptualization, L.L.; Methodology, L.L.; Software, Z.C.; Validation, L.L., Z.C. and P.F.; Formal Analysis, L.L.; Investigation, L.L., Z.C. and P.F.; Writing–Original Draft Preparation, L.L.; Writing–Review & Editing, L.L.; Supervision, L.L.; Funding Acquisition, L.L.

**Funding:** This work is supported by the National Natural Science Foundation of China (No. 51605084 and U1708265) and the Fundamental Research Funds for the Central Universities of China (N170304019 and N170308028).

**Conflicts of Interest:** The authors declare no conflict of interest.

## References

- Garcia-Junceda, A.; Capdevila, C.; Caballero, F.G.; Garcia de Andres, C. Dependence of martensite start temperature on fine austenite grain size. *Scr. Mater.* **2008**, *58*, 134–137. [[CrossRef](#)]
- Morito, S.; Saito, H.; Ogawa, T.; Furuhashi, T.; Maki, T. Effect of austenite grain size on the morphology and crystallography of lath martensite in low carbon steels. *ISIJ Int.* **2005**, *45*, 91–94. [[CrossRef](#)]
- Furuhashi, T.; Kikumoto, K.; Saito, H.; Sekine, T.; Ogawa, T.; Morito, S.; Maki, T. Phase transformation from fine-grained austenite. *ISIJ Int.* **2008**, *48*, 1038–1045. [[CrossRef](#)]
- Hanamura, T.; Torizuka, S.; Tamura, S.; Enokida, S.; Takechi, H. Effect of austenite grain size on transformation behavior, microstructure and mechanical properties of 0.1C-5Mn martensitic steel. *ISIJ Int.* **2013**, *53*, 2218–2225. [[CrossRef](#)]
- Hidalgo, J.; Santofimia, M.J. Effect of prior austenite grain size refinement by thermal cycling on the microstructural features of as-quenched lath martensite. *Metall. Mater. Trans. A* **2016**, *47*, 5288–5301. [[CrossRef](#)]
- Matsuzaki, A.; Bhadeshia, H.K.D.H. Effect of austenite grain size and bainite morphology on overall kinetics of bainite transformation in steels. *Mater. Sci. Technol.* **1999**, *15*, 518–522. [[CrossRef](#)]
- Rees, G.I.; Bhadeshia, H.K.D.H. Bainite transformation kinetics Part 1 Modified model. *Mater. Sci. Technol.* **1992**, *8*, 985–993. [[CrossRef](#)]
- Lan, L.Y.; Qiu, C.L.; Zhao, D.W.; Gao, X.H.; Du, L.X. Effect of austenite grain size on isothermal bainite transformation in low carbon microalloyed steel. *Mater. Sci. Technol.* **2011**, *27*, 1657–1663. [[CrossRef](#)]
- Shome, M.; Gupta, O.P.; Mohanty, O.N. Effect of simulated thermal cycles on the microstructure of the heat-affected zone in HSLA-80 and HSLA-100 steel plates. *Metall. Mater. Trans. A* **2004**, *35*, 985–996. [[CrossRef](#)]
- Lee, S.J.; Park, J.S.; Lee, Y.K. Effect of austenite grain size on the transformation kinetics of upper and lower bainite in a low-alloy steel. *Scr. Mater.* **2008**, *59*, 87–90. [[CrossRef](#)]
- Lan, L.Y.; Qiu, C.L.; Zhao, D.W.; Gao, X.H.; Du, L.X. Effect of reheat temperature on continuous cooling bainite transformation behavior in low carbon microalloyed steel. *J. Mater. Sci.* **2013**, *48*, 4356–4364. [[CrossRef](#)]
- abbasi, M.; Nelson, T.W.; Sorensen, C.D. Analysis of variant selection in friction-stir-processed high-strength low-alloy steels. *J. Appl. Crystallogr.* **2013**, *46*, 716–725. [[CrossRef](#)]
- Lan, L.Y.; Kong, X.W.; Qiu, C.L. Characterization of coarse bainite transformation in low carbon steel during simulated welding thermal cycles. *Mater. Charact.* **2015**, *105*, 95–103. [[CrossRef](#)]
- Zhao, H.; Wynne, B.P.; Palmiere, E.J. Effect of austenite grain size on the bainitic ferrite morphology and grain refinement of a pipeline steel after continuous cooling. *Mater. Charact.* **2017**, *123*, 128–136. [[CrossRef](#)]
- Garcia de Andres, C.; Caballero, F.G.; Capdevila, C.; Alvarez, L.F. Application of dilatometric analysis to the study of solid-solid phase transformations in steels. *Mater. Charact.* **2002**, *48*, 101–111. [[CrossRef](#)]

16. Chen, X.W.; Qiao, G.Y.; Han, X.L.; Wang, X.; Xiao, F.R.; Liao, B. Effects of Mo, Cr and Nb on microstructure and mechanical properties of heat affected zone for Nb-bearing X80 pipeline steels. *Mater. Des.* **2014**, *53*, 888–901. [[CrossRef](#)]
17. Lan, L.Y.; Yu, M.; Qiu, C.L. On the local mechanical properties of isothermally transformed bainite in low carbon steel. *Mater. Sci. Eng. A* **2019**, *742*, 442–450. [[CrossRef](#)]
18. Li, X.D.; Shang, C.J.; Ma, X.P.; Gault, B.; Subramanian, S.V.; Sun, J.B.; Misra, R.D.K. Elemental distribution in the martensite-austenite constituent in intercritically reheated coarse-grained heat-affected zone of a high-strength pipeline steel. *Scr. Mater.* **2017**, *139*, 67–70. [[CrossRef](#)]
19. Biss, V.; Cryderman, R.L. Martensite and retained austenite in hot-rolled low-carbon bainitic steel. *Metall. Mater. Trans.* **1971**, *2*, 2267–2276. [[CrossRef](#)]
20. Zhang, M.X.; Kelly, P.M. Determination of carbon content in bainitic ferrite and carbon distribution in austenite by using CBKLD. *Mater. Charact.* **1998**, *40*, 159–168. [[CrossRef](#)]
21. Tomozawa, M.; Miyahara, Y.; Kako, K. Solute segregation on  $\Sigma 3$  and random grain boundaries in type 316L stainless steel. *Mater. Sci. Eng. A* **2013**, *578*, 167–173. [[CrossRef](#)]
22. Thibaux, P.; Metenier, A.; Xhoffer, C. Carbon diffusion measurement in austenite in the temperature range 500 to 900 °C. *Metall. Mater. Trans. A* **2007**, *38*, 1169–1176. [[CrossRef](#)]
23. Escobar, J.D.; Faria, G.A.; Wu, L.; Oliveira, J.P.; Mei, P.R.; Ramirez, A.J. Austenite reversion kinetics and stability during tempering of a Ti-stabilized supermartensitic stainless steel: Correlative in situ synchrotron X-ray diffraction and dilatometry. *Acta Mater.* **2017**, *138*, 92–99. [[CrossRef](#)]
24. Wan, X.L.; Wu, K.M.; Nune, K.C.; Li, Y.; Cheng, L. In situ observation of acicular ferrite formation and grain refinement in simulated heat affected zone of high strength low alloy steel. *Sci. Technol. Weld. Join.* **2015**, *20*, 254–263. [[CrossRef](#)]
25. Sainis, S.; Farahani, H.; Gamsjager, E.; van der Zwaag, S. An In-situ LSCM study on bainite formation in a Fe-0.2C-1.5Mn- 2.0Cr alloy. *Metals* **2018**, *8*, 498–512. [[CrossRef](#)]
26. Takayama, N.; Miyamoto, G.; Furuhashi, T. Effects of transformation temperature on variant pairing of bainitic ferrite in low carbon steel. *Acta Mater.* **2012**, *60*, 2387–2396. [[CrossRef](#)]
27. Borgenstam, A.; Hillert, M.; Agren, J. Metallographic evidence of carbon diffusion in the growth of bainite. *Acta Mater.* **2009**, *57*, 3242–3252. [[CrossRef](#)]
28. Slane, J.A.; Wolvertson, C.; Gibala, R. Experimental and theoretical evidence for carbon-vacancy binding in austenite. *Metall. Mater. Trans. A* **2004**, *35*, 2239–2245. [[CrossRef](#)]
29. Abe, T.; Tsukada, K.; Tagawa, H.; Kozasu, I. Grain boundary segregation behavior of phosphorus and carbon under equilibrium and non-equilibrium conditions in austenitic region of steels. *ISIJ Int.* **1990**, *30*, 444–450. [[CrossRef](#)]
30. Timokhina, I.B.; Liss, K.D.; Raabe, D.; Rakha, K.; Beladi, H.; Xiong, X.Y.; Hodgson, P.D. Growth of bainitic ferrite and carbon partitioning during the early stages of bainite transformation in a 2 mass% silicon steel studied by in situ neutron diffraction, TEM and APT. *J. Appl. Crystallogr.* **2016**, *49*, 399–414. [[CrossRef](#)]
31. Kempen, A.T.W.; Sommer, F.; Mittemeijer, E.J. The kinetics of the austenite-ferrite phase transformation of Fe-Mn: Differential thermal analysis during cooling. *Acta Mater.* **2002**, *50*, 3545–3555. [[CrossRef](#)]
32. Song, T.; Cooman, B.C.D. Effect of boron on the isothermal bainite transformation. *Metall. Mater. Trans. A* **2013**, *44*, 1686–1705. [[CrossRef](#)]
33. Madariaga, I.; Gutierrez, I. Role of the particle-matrix interface on the nucleation of acicular ferrite in a medium carbon microalloyed steel. *Acta Mater.* **1999**, *47*, 951–960. [[CrossRef](#)]

